Clays and Clay Minerals, Vol. 48, No. 5, 537–548, 2000.

GEOLOGY AND CHARACTERIZATION OF TWO HYDROTHERMAL NONTRONITES FROM WEATHERED METAMORPHIC ROCKS AT THE ULEY GRAPHITE MINE, SOUTH AUSTRALIA

JOHN L. KEELING,[1] MARK D. RAVEN,[2] AND WILL P. GATES[2]

[1] Primary Industries and Resources, South Australia, GPO Box 1617 Adelaide, SA 5001 Australia
[2] CSIRO Land and Water, PMB No. 2, Glen Osmond, SA 5064 Australia

Abstract—Mining operations during the early 1990s at Uley Graphite Mine near Port Lincoln on southern Eyre Peninsula, South Australia, uncovered abundant nontronite veins in deeply weathered granulite facies schist, gneiss, and amphibolite of Palaeoproterozoic age. Two types of nontronite are present: a bright yellowish-green clay (NAu-1) distributed as veinlets and diffuse alteration zones within kaolinized schist and gneiss, and a massive to earthy, dark-brown clay (NAu-2) infilling fracture networks mainly in amphibolite or basic granulite. The nontronites are the product of low-temperature hydrothermal alteration of primary minerals, biotite, and amphibole. The principal chemical difference between NAu-1 and NAu-2 is a higher alumina content in NAu-1, which was either inherited during hydrothermal alteration of biotite in the host rock or acquired through recrystallization of nontronite during subsequent weathering and associated kaolinization. Sufficient bulk samples of both NAu-1 and NAu-2 were collected to supplement reference nontronite of the Source Clay Repository of The Clay Minerals Society. The clay fraction of the bulk samples is typically >85%. NAu-1 contains minor kaolin and quartz which are easily removed to give a high purity nontronite of composition $M^{+}_{1.05}[Si_{6.98}Al_{1.02}][Al_{0.29}Fe_{3.68}Mg_{0.04}]O_{20}(OH)_4$, similar to that of nontronite from Garfield, Washington. NAu-2 contains fewer total impurities but the presence of trace amounts of submicron carbonate and iron oxyhydroxide requires additional chemical treatment to produce a nontronite of purity comparable to NAu-1. Composition of NAu-2 was calculated as $M^{+}_{0.72}[Si_{7.55}Al_{0.45}][Fe_{3.83}Mg_{0.05}]O_{20}(OH)_4$, although infrared data indicate that at least some Fe is in tetrahedral coordination.

Key Words—Amphibole Alteration, Biotite Alteration, Hydrothermal Alteration, Infrared Spectroscopy, NAu-1, NAu-2, Nontronite, Weathering, X-ray Diffraction.

INTRODUCTION

Nontronite is a swelling 2:1 phyllosilicate and represents the ferric endmember within the nontronite-beidellite series. Nontronite is not common but it does have a widespread occurrence in both terrestrial and oceanic environments, usually as weathering or hydrothermal alteration products of Fe-rich silicates (Ross and Hendricks, 1945; Eggleton, 1975; Bender Koch *et al.*, 1995) or as authigenic deposits precipitated from hydrothermal fluids at sites of active sea-floor spreading (Bischoff, 1972; Murnane and Clague, 1983; Köhler *et al.*, 1994). Although nontronite has been studied extensively, it continues to attract a high level of research interest owing primarily to high iron content. The high iron content is suitable for investigation by a wide range of spectroscopic techniques that complements traditional diffraction studies (Goodman *et al.*, 1976; Besson *et al.*, 1983; Cardile and Johnston, 1985; Manceau *et al.*, 1998).

Research supplies of uniform reference nontronite are diminishing. The Source Clays Repository of The Clay Minerals Society recently expired the stocks of NG-1 nontronite and supplies of ferruginous smectite, SWa-1, are low. Another problem is the inconsistency in chemical analyses, structural formulae, and related interpretation of spectroscopic and structural data for nontronites. For example, nontronite from Garfield, Whitman Co., Washington (API H33a) is reported with widely differing chemical analyses and structural formulae thereby producing a wide disparity of conclusions relating to spectroscopic data (*e.g.*, see Goodman *et al.*, 1976; Eggleton, 1977; Besson *et al.*, 1983; Bonnin *et al.*, 1985; Murad *et al.*, 1990; Manceau *et al.*, 1998). To augment reference materials, we have collected bulk samples of two nontronites from the Uley Graphite Mine in South Australia.

Uley Mine is located 18 km west-southwest of Port Lincoln on southern Eyre Peninsula, South Australia (Figure 1). Graphite mineralization was discovered in the 1910s, and the mine has operated intermittently since the late 1920s. Exploration during the 1980s led to reopening the mine from 1986 to 1993 when, after a sharp decline in world graphite prices in 1992, the operation was placed on care and maintenance. Indicated resources at Uley are 2.9 million tons (Mt) of grade 13% graphitic carbon which include 1.5 Mt at 15% graphite (McNally, 1997). Total resources of some 350 Mt at 6–7% graphite are inferred from geophysical surveys and drilling around Uley and at four nearby prospects, making this the largest recorded graphite resource in Australia.

The presence of bright-green to yellow-green clay was found in drill holes and encountered during min-

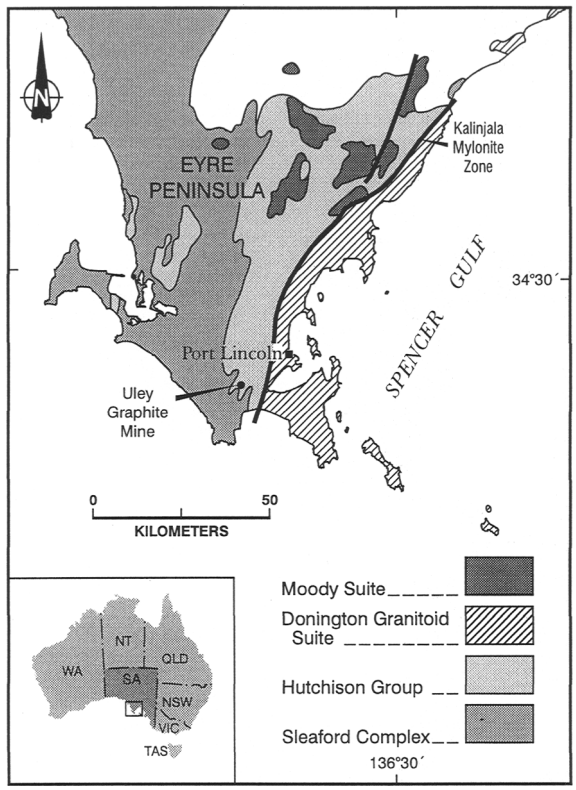

Figure 1. Simplified geology of Eyre Peninsula showing location of Uley Graphite Mine (modified from Drexel *et al.*, 1993).

ing at ~15 m below original ground surface. X-ray diffraction (XRD) of <2-μm size fraction confirmed that the clay was dominantly nontronite. A stiff, dark-brown clay forming veins and masses in the eastern lower pit face was shown also to be dominantly nontronite. Purification of the smectite component produced high yields of nearly pure nontronite. Bulk samples of the two clays were collected as potential reference materials and submitted for inclusion in The Clay Minerals Society's Source Clays Repository.

In this paper, we describe the geological setting of the Uley Graphite Mine and the nontronite occurrence. The mineralogy of bulk clays as supplied to the Source Clays Repository is given together with preliminary characterization of nontronite refined from these samples. Additional spectroscopic, chemical, and structural characterization of Uley nontronites is in progress.

GEOLOGY

The Uley Graphite Mine is located on the southern margin of the Gawler Craton, an area of crystalline basement of Archaean to Mesoproterozoic age. Graphite mineralization, as disseminated crystalline flake graphite, is hosted within a sequence of predominantly schist and gneiss correlated with Cook Gap Schist in the Middleback Subgroup, Hutchison Group of Palaeoproterozoic age (~1900–1850 Ma). Ore horizons (>6% graphite) are ≤12 m thick and are largely stratigraphically controlled, being high-grade metamorphic equivalents of original carbonaceous-rich sediments (Taylor and Berry, 1990). Basic igneous rocks occur within the stratigraphic sequence and represent either mafic volcanics or intrusive gabbro/dolerite sills and dikes that were largely transposed into regional structural concordance during isoclinal folding (Parker, 1993).

Three periods of metamorphism and deformation are generally recognized in the Hutchison Group metasediments and these are collectively assigned to the Kimban Orogeny (~1800–1600 Ma). The first and second metamorphic events were the most intense, reaching an estimated maximum of 700–900 MPa and 800–850°C on southern Eyre Peninsula (Bradley, 1980; Parker, 1993). The third event was less intense in metamorphic grade, reaching lower amphibolite facies, but it was a significant deformational event (D3) responsible for the formation of broad north-south regional folds and major shear zones. The Uley Mine is located near the hinge of a regional D3 anticline in which asymmetric, tight to isoclinal mesofolds produce local thickening of graphitic horizons.

After metamorphism, hydrothermal activity produced minor fracture-filling quartz veinlets containing traces of iron and copper sulfides, and rare thin coatings and veinlets of celadonite. Crystalline basement rocks at Uley are extensively altered by weathering such that silicate minerals in the upper 10–15 m were mostly altered to clay minerals and iron oxide minerals. Clay alteration products persist to >60 m depth. The age of onset of weathering is uncertain, but regional studies indicate extensive weathering prior to Middle Eocene times (Benbow *et al.*, 1995) with widespread preservation of weathered profiles in basement terranes.

During Pleistocene times, lower sea levels exposed coastal marine carbonate sediments to erosion by deflation with the resulting products blown inland to form calcareous dunefields that cover large areas of western and southern Eyre Peninsula. Inland, the dunes were fixed by vegetation and subsequent dissolution and precipitation has redistributed carbonate within the dunes and the underlying weathered bedrock.

Uley Mine

During the 1986–93 mining campaign, an open pit, 120 by 100 by 20 m depth, was excavated in graphite ore forming the hinge zone of a north-northeasterly plunging anticline. The excavation exposes the most weathered portion of the orebody where much of the original textural variation and structural relationships between lithologies are obliterated. Despite the extent

https://doi.org/10.1346/CCMN.2000.0480506 Published online by Cambridge University Press

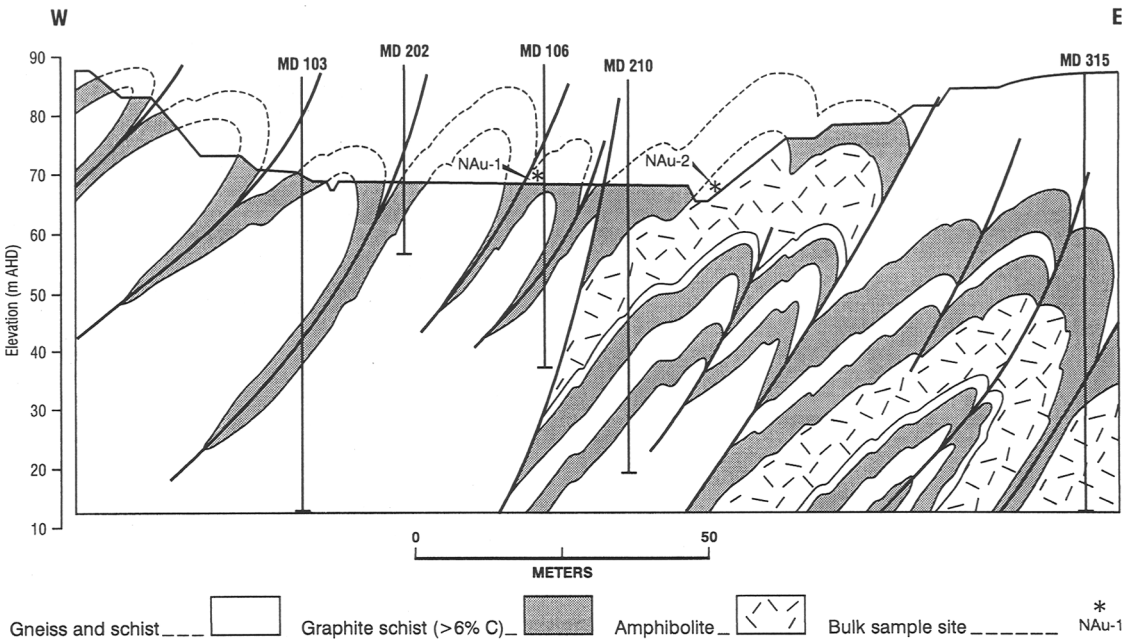

Figure 2. Geological section of the Uley Graphite Mine through the main pit showing location of nontronite bulk-sample sites and drill hole MD 210.

of weathering, geological structures can be traced, particularly on the southern pit faces, which show a series of tightly folded gneissic and graphitic schistose units that form part of an anticlinorium in which the synclinal folds are often attenuated by shearing along graphitic layers (Figure 2). Disseminated crystalline flake graphite is ubiquitous but economic concentrations (>6% graphite) are associated with particular lithologies, typically quartz-biotite schist or medium to coarse-grained quartz-feldspar-biotite ± garnet gneiss. Rock fabric and mineralogy indicate that metamorphic grade reached upper amphibolite to lower granulite facies. Graphite production was principally from an 8–12-m thick sequence of highly weathered biotite-quartz-graphite schist with finely interlayered gneissic bands and lenses. On the eastern side of the pit, the main graphite sequence overlies a 10–15-m thick weathered amphibolite (Figure 2) below which further graphite schist units were identified by drilling. At cessation of mining in 1993, the pit floor was at elevation 67.5 m, ~19 m below original ground surface. No further significant earthworks had taken place prior to the collection of samples in March 1998.

MATERIALS AND METHODS

Bulk samples of NAu-1 were collected from the pit floor in kaolinized schist in the central area of the open cut (Figure 2). NAu-2 was collected from weathered amphibolite exposed near the base of the eastern pit wall in a 3-m deep drain excavated at the perimeter of the pit floor. A total of ~120 kg of each clay was collected to produce six 20-L drums of a bright-green clay (Munsell colour 5GY6/6) and six 20-L drums of a dark-brown clay (Munsell colour 10YR2/1).

The weathered profile and the distribution of nontronite were investigated by quantitative mineral analyses of vertical drill hole, MD 210, which was core drilled to 66.2 m (Figures 2 and 3), and by examination of exposures in the pit. Inspection of MD 210 showed significant amounts of nontronite below the present pit floor level. A continuous thin slice was sampled, crushed, and bagged over ~1-m intervals, with small adjustments in sample intervals to account for major lithological changes and intervals of poor core recovery. In total, 57 samples were collected. The entire sample for each interval was ground in a tungsten carbide ring mill and a sample taken for quantitative XRD (see below). Preferred orientation made graphite difficult to quantify by XRD. Graphite content of samples was determined by the Leco furnace method (Yeomans and Bremer, 1991) after treatment with HCl to remove carbonate.

For scanning electron microscopy (SEM), nontronite and associated minerals were collected from the two bulk-sample sites. Dry (105°C) fragments were mounted on aluminum stubs and coated with 30 nm of carbon. These were examined in secondary electron mode using a Cambridge Stereoscan S250 scanning electron microscope with a LINK system energy dispersive X-ray (EDX) analyzer.

For nontronite characterization, a representative sample was taken from each of the 20-L drums con-

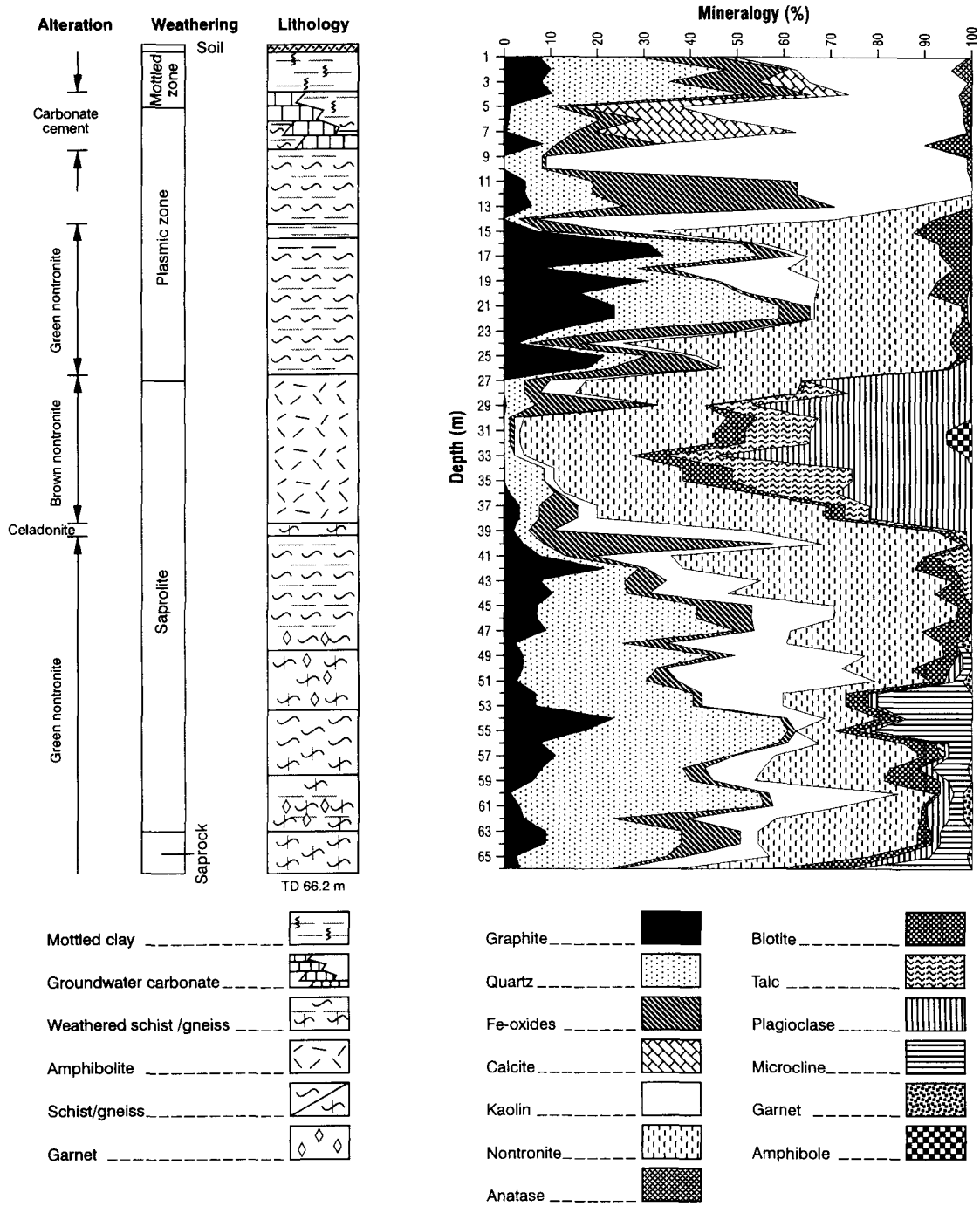

Figure 3. Summary of alteration, weathering, lithology, and mineralogy of drill hole MD 210.

taining bulk NAu-1 and NAu-2. The 12 samples were oven dried at 105°C overnight. Each was separated into four particle size ranges: <0.2, 0.2–0.5, 0.5–2, and >2 μm, using NaCl to disperse the clay and centrifugation to separate the size fractions. The separated fractions were Ca-saturated, washed, and dried. Oven-dried bulk samples and separated size fractions were gently ground by hand using an agate mortar and pestle and lightly back pressed to reduce orientation effects, into steel sample holders for XRD analysis. Diffraction patterns were collected using a Philips PW1800 microprocessor-controlled diffractometer using CoKα radiation, a variable divergence slit, and a graphite monochromator. The diffraction data were re-

https://doi.org/10.1346/CCMN.2000.0480506 Published online by Cambridge University Press

corded in steps of 0.05 °2θ with a 1.0-s counting time per step.

Quantitative mineralogy was determined from XRD patterns using full-profile Rietveld refinement based on calculated and standard profiles in SIROQUANT software (Taylor, 1991; Taylor and Matulis, 1994). Raw data were modified first by subtracting the background and by re-calibration of intensity for the variable divergence slit. This Rietveld technique was used also to estimate the relative proportions of minerals present in the 57 bulk samples from core MD 210.

The <0.2-μm sample fractions were ignited to 1050°C for 1 h and major elements determined by the X-ray fluorescence (XRF) method of Norrish and Hutton (1969) using a Philips PW1480 wavelength dispersive XRF spectrometer. Infrared (IR) spectra were collected on KBr pressed disks of the Ca-saturated <0.2-μm size fractions of both nontronites (applied pressure of 9 tons; ~1.5 mg clay and 150 mg KBr) using a Biorad 175C Fourier-transform spectrophotometer equipped with CsI beamsplitter and with a dry-air purge. Transmission spectra were collected over the wavenumber range of 350–4000 cm^{-1} (2 cm^{-1} resolution, Happ-Genzel apodization). The results showed trace amounts of other mineral phases. To obtain purified material for XRF analysis, samples were further separated to the <0.15-μm size fractions after Li saturation (Goodman *et al.,* 1976). IR spectra of the <0.15-μm fractions showed that the contaminant phase in NAu-1 was removed but for NAu-2, separation of the <0.15-μm size fraction resulted in concentration of Mg/Mn-rich carbonate. This was removed by treatment with 0.1 M acetic acid. Chemical composition of the purified samples was then determined by XRF.

RESULTS

Nontronite distribution

Drill hole MD 210. Owing to the presence of highly weathered rock, and the limited exposures of nontronite (<6 m) at the pit, drill hole MD 210 (Figure 3) was examined in detail. Core samples show the effects of weathering extend to >60 m depth. Four zones of weathering were recognized, mottled, plasmic, saprolite, and saprock (Figure 3), based on degree of alteration of minerals and of primary rock structures. The mottled zone is 3.6 m thick of dominantly kaolinitic clay mottled red-brown, yellow-brown, white, and gray with a well-developed pedogenic fabric. Throughout the mottled zone are minor white to pale-yellow carbonate concentrations as irregular hard nodules or friable patches to 60 mm across. Fine-grained graphite stringers and patches of coarse-grained quartz indicate that the mottled zone developed within crystalline rock. Dominant kaolin, quartz, and iron oxides are present with variable but lesser amounts of calcite, graphite, and anatase.

The plasmic zone from 3.9 to 26.6 m has >80% of weatherable minerals altered to clay and much of the original rock fabric destroyed. The upper section between 3.9–8.2 m is further modified by pervasive carbonate precipitated from groundwater to form crystalline white patches of massive to vuggy calcite that replace or cement quartz grains and kaolin. The interval from 8.2 to 14.2 m is dominantly goethite with minor hematite, kaolin, quartz, and 5% graphite. At 14 m, the first appearance of yellow-green nontronite (NAu-1) occurs as waxy patches ≤10 mm across and as wispy anastomosing veinlets in a mixture of white and orange-brown kaolin. Green nontronite (NAu-1) is the dominant mineral phase from 14.7 to 15.4 m and it is intimately mixed with iron oxide, kaolin, and graphite to form a fine-grained speckled, orange-brown, green, and gray rock. At 15.4 m, the main graphite orebody was encountered as weathered graphite schist with minor gneissic bands represented by coarse quartz in a white kaolin matrix. Graphite grade across the 11.2-m thick ore intersection from 15.4 to 26.6 m varies from 3 to 34% C. Quartz content is ~20% and remnant biotite is present throughout, much of which shows alteration to iron oxides and clay minerals, dominantly nontronite. Green to yellow-green nontronite as veinlets and patches comprises ~30% of the graphite ore zone. Between 23–24.8 m, nontronite content increases to >50% corresponding to an interval of low graphite grade of 3.2% C. Associated minerals are kaolin, goethite, and traces of quartz and biotite. From 24.8 to 26.6 m, Fe-oxide content increases sharply from 7 to 25%, accompanied by an increase in graphite grade to 18–20% C and a coarsening of graphite flake size to 4 mm. Over this interval, nontronite is present as a mixture of pale-yellow and green clay.

The top of the saprolite zone, at 27 m, coincides with a lithological change from schist to altered amphibolite. The amphibolite is a friable, white to pale-brown, medium-grained, equigranular rock composed of a mixture of calcic plagioclase and nontronite with minor Fe-rich oxides, talc, and kaolin, and traces of biotite, quartz, and amphibole. Classification of the rock as an amphibolite was based on feldspar composition and textural similarities with relatively fresh crystalline mafic rock, from deeper intersections in earlier exploration holes, that comprise dominantly hornblende and Ca-rich plagioclase with trace amounts of clinopyroxene, biotite, and orthopyroxene (D. Mason, unpublished data, 1997). The thickness of the amphibolite intersection in MD 210 is ~12 m. The rock contains negligible graphite. In the upper 2 m of the amphibolite, nontronite (NAu-2) forms veinlets and bands 5–30 mm wide as an earthy yellow-brown to dark-brown clay mixed with 3–25% goethite. At 30.7

m, a 0.2-m band of relatively pure nontronite was intersected and at 33.7 m, there is a 0.5-m mass of dominantly nontronite veins. Here, nontronite is dark-brown to black and ranges from earthy and dull, to stiff compact masses displaying fibrous surface striations and a resinous luster. Minor coarse, shiny black biotite flakes are present and XRD data show both an increase in talc content and the presence of minor amounts of amphibole. Throughout the altered amphibolite, nontronite content averages 35% and is distinct both in color and character from the yellow-green nontronite intersected higher in the drill hole.

The base of the amphibolite at ~38 m is marked by an increase in kaolin (40%), disappearance of plagioclase, reappearance of patches of bright yellow-green nontronite (NAu-1), and traces of dark bluish-green celadonite. At 39.2 m, an Fe-rich oxide-cemented schist band was intersected followed by altered graphite schist and fine-grained graphite gneiss from 39.7 to 42.7 m. Clay minerals are still dominant in this section, primarily bright-green nontronite (30–50%) and kaolin (10–20%) together with quartz and minor biotite. Significant amounts of graphite are present at 53.2–58.5 m and this rock contains less total clay, ~30% (nontronite + kaolin), with higher quartz content (30–50%) together with K-rich feldspar and some plagioclase and garnet.

The assignment of the saprock/saprolite boundary at 63 m was based largely on the presence of a comparatively solid, competent gneiss. Nontronite, kaolin, and iron oxides persist to the full depth of the drill hole at 66.2 m but alteration is increasingly patchy and restricted. Grayish-green to yellow-green nontronite is present as veinlets and fracture filling and commonly forms patches in biotite-rich bands.

Pit-floor samples. Nontronite in the pit floor at ~19–22 m below the original pit surface (Figure 2) occurs in highly altered rock. NAu-1 is associated with kaolinized schist near the base of a graphite schist unit. Although 5–40-mm thick veins of waxy NAu-1 were encountered, the nontronite is mainly as diffuse grayish-green masses in kaolin and commonly includes areas of fine-grained, silver-gray mica. Coarse books of yellow-brown to dark-brown biotite are also present as scattered crystals or concentrated in weakly defined bands within nontronite masses. Veins and masses of NAu-1 commonly include blocky friable aggregates of iron oxide usually concentrated in the central region of the vein or mass. In some nontronite veins, black manganese oxide (possibly vernadite based on XRD) is a common coating on fracture surfaces.

NAu-2 was taken from a network of intersecting fractures that enclose patches of medium to coarse-grained sandy Ca-rich feldspar that had undergone physical weathering but not extensive kaolinization. Rock textures of gneissic fabric and joints are weakly preserved in the friable rock which is interpreted as an amphibolite or basic granulite where the majority of the ferromagnesian minerals were removed through dissolution. Nontronite in 10–50-mm veins is most persistent along planes parallel to metamorphic banding and fills joints and crosscutting fractures. At some vein intersections, large masses of compact, dark-brown nontronite were collected showing adamantine to dull luster, in part coated by an earthy, yellow-brown clay.

Electron microscopy

Samples prepared from areas of relatively pure nontronite showed curved flakes 2–5 μm across with slightly crumpled edges, typical of smectite crystal aggregates. NAu-1 and NAu-2 were not markedly different at magnifications with the SEM of 20–30,000×. NAu-2 overall appeared to be more compact with slightly smaller but thicker flakes compared to NAu-1 (Figure 4). Comparative compositions of nontronite, based on EDX analysis of individual flakes, showed that NAu-2 was consistently higher in Fe and lower in Al compared with NAu-1. Small amounts of Ca and Mg were present in both clays and it is assumed that Ca^{2+} is the dominant exchangeable cation in untreated samples.

Primary mineral phases associated with the two nontronites were different and reflected host lithology. In the area where NAu-1 was sampled, biotite was the remnant primary mineral and the focus of the SEM study. Biotite grains, as fine to coarse flakes 100–400 μm across, varied from moderately fresh to highly altered. Alteration took place preferentially along individual mica layers, parallel to cleavage, with progressive conversion of biotite to nontronite (Figure 5). Kaolinite was observed as micron-sized crystals projecting from the edge of biotite cleavage sections and as broad ragged-edged sheets dislodged from mica cleavage surfaces (Figure 5b). Both kaolinite and green nontronite were apparent products of biotite alteration, but the data to determine relative timing of formation of the two clay minerals was inconclusive.

Remnant rock fragments enclosed within veinlets of NAu-2 comprised a high proportion of mostly intact grains of Ca-rich plagioclase showing variable development of surface etch pits. Nontronite was observed coating surfaces of plagioclase grains and partly filling etch pits and dissolution features, especially in more altered grains (Figure 6). Ca-rich amphibole, of composition approximating alumino-ferro-hornblende (EDX analyses), was usually restricted to the central portion of rock fragments, away from areas of high nontronite concentration. Most grains examined showed extensive dissolution via crystallographically controlled etch pits (Figure 7) resulting in cavernous voids lined with sharp dentate projections, a common characteristic of advanced amphibole weathering (*e.g.*,

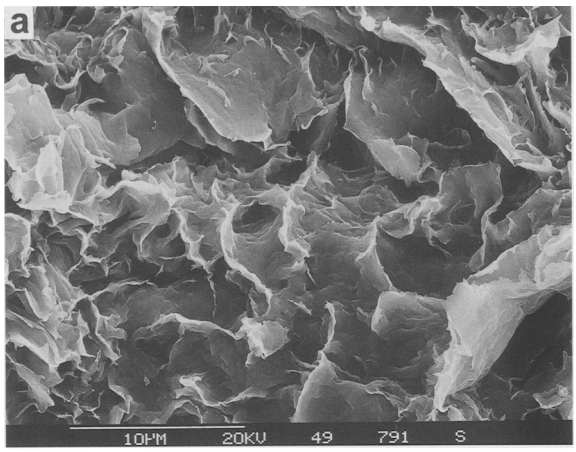

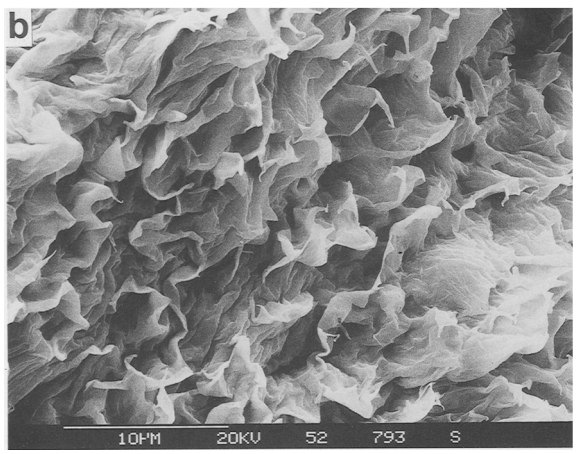

Figure 4. Secondary electron images of selected fragments of nontronite taken from bulk clay samples (a) NAu-1, green nontronite flakes of ≤20 μm across, (b) NAu-2, brown nontronite as slightly smaller crystal aggregates with more compact habit relative to NAu-1. Scale bar on both micrographs is 10 μm.

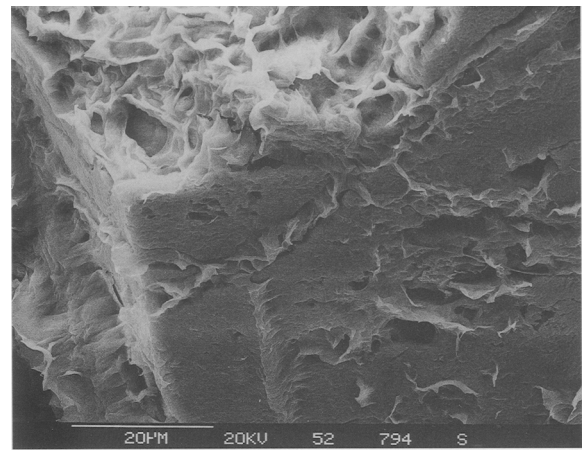

Figure 6. Secondary electron image of calcic plagioclase from altered amphibolite from the bulk sample site for NAu-2. Plagioclase shows development of etch pits partly coated and filled by brown nontronite.

Berner and Schott, 1982; Anand and Gilkes, 1984; Velbel, 1989). Although clay products were observed as thin coatings on the surface of some amphibole grains, voids formed by dissolution were typically clean and free of any obvious secondary crystallization products (Figure 7). Accessory coarse biotite, >1 mm across, was present with amphibole and formed blocky, compact crystals showing slight splaying of cleavage sections with the edges of mica layers showing minor alteration to smectite.

Mineralogy of bulk samples

Both NAu-1 and NAu-2 gave a high yield of clay-sized fraction, >85% of the <2-μm size fraction, of which nearly 90% was <0.2 μm in size and nearly pure nontronite (Tables 1 and 2). Other crystalline phases present in bulk samples of NAu-1 were kaolin,

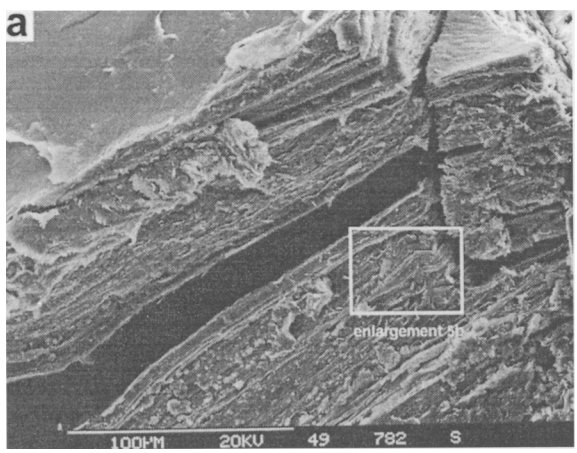

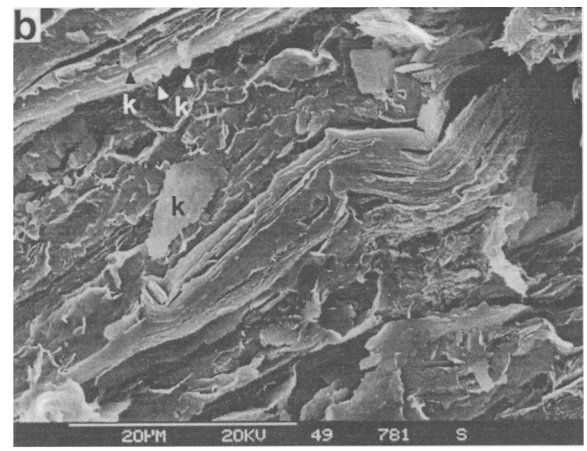

Figure 5. Secondary electron image of biotite present with NAu-1 showing (a) largely intact biotite flake in which some layers have altered to green nontronite, (b) detail of (a) showing biotite largely altered to nontronite, but also with kaolinite (k) as flakes and as small crystals (arrows) protruding from the edge of the biotite cleavages.

https://doi.org/10.1346/CCMN.2000.0480506 Published online by Cambridge University Press

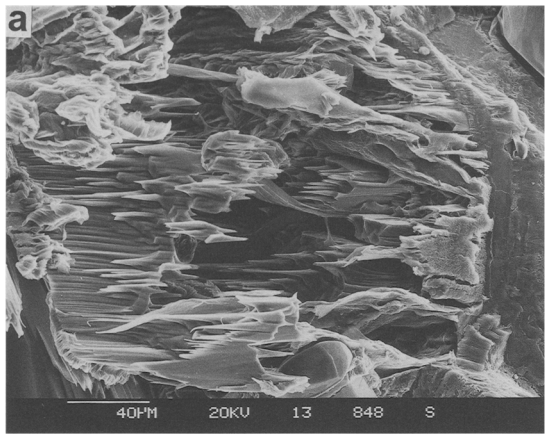

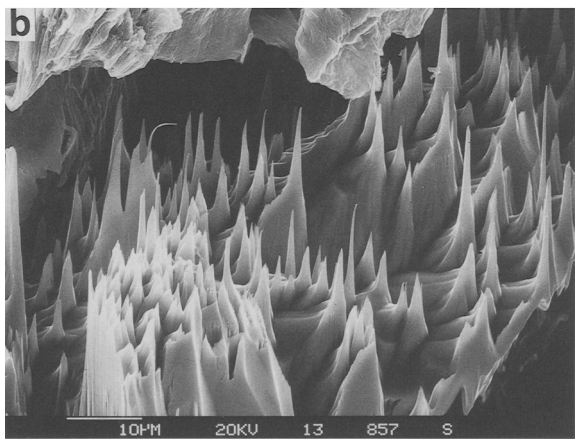

Figure 7. Secondary electron images of hornblende associated with sample NAu-2 showing (a) a high degree of crystallographically controlled dissolution, (b) distinctive dentate projections with clean etch surfaces and little or no alteration products near the site of dissolution.

quartz, biotite, and goethite and for NAu-2, minor plagioclase with trace amounts of quartz, biotite, talc, and ilmenite (Table 2; Figure 8). Mineralogy typical of various size fractions of NAu-1 and NAu-2 is shown in Table 2. Diffraction patterns for the <0.2-µm size fractions are shown in Figure 9.

A feature of oven-dried NAu-2 was the presence, after drying, of two broad XRD peaks at ~13.7 and 10.0 Å (Figure 8). The 10-Å peak is related to dehydrated samples, and the 13-Å peak is related to a single H_2O plane in the interlayer (single-layer hydration state). Complete rehydration was not possible. After

Table 1. Particle-size data for bulk nontronite samples (average of six samples).

Sample	>2 µm	0.5–2 µm	0.2–0.5 µm	<0.2 µm
NAu-1	8 ± 5%	4 ± 2%	6 ± 3%	82 ± 9%
NAu-2	5 ± 2%	5 ± 1%	9 ± 2%	82 ± 3%

Table 2. Mineralogical composition of NAu-1 and NAu-2.

	Bulk	>2 µm	0.5–2 µm	0.2–0.5 µm	<0.2 µm
		NAu-1			
Nontronite	90	49	86	93	>99
Kaolin	4	4	7	4	bd
Quartz	2	13	1	<1	bd
Biotite	<1	2	1	bd	bd
Goethite	3	31	5	3	bd
		NAu-2			
Nontronite	95	10	83	99	>99
Plagioclase	5	68	10	bd	bd
Quartz	<1	10	2	<1	bd
Biotite	bd	4	bd	bd	bd
Talc	bd	3	5	bd	bd
Ilmenite	bd	5	bd	bd	bd

bd = below detection.

redispersion in water and gently air-drying, the diffraction pattern reverted to the two-layer hydration state (~15 Å). However, some (<5%) dehydrated (10 Å) layers persisted. By contrast, NAu-1 rehydrated to the two-layer hydration state by allowing the clay to equilibrate overnight at ambient laboratory conditions.

Chemistry

Major oxide chemistry for the purified <0.15-µm size fraction of Ca-saturated samples of NAu-1 and NAu-2 are given in Table 3. NAu-2 showed higher Fe_2O_3 (37.9%) and lower Al_2O_3 (3.1%) than NAu-1 (Fe_2O_3 35.9% and Al_2O_3 8.2%). These data were used to calculate structural formula using CLAYFORM (Bodine, 1987). Insignificant levels of TiO_2, MnO, and P_2O_5 were assumed to be related to impurities and excluded from the calculations to give the following structural formula: NAu-1, $M^{+}_{1.05}[Si_{6.98}Al_{1.02}][Al_{0.29}Fe_{3.68}Mg_{0.04}]O_{20}(OH)_4$; NAu-2, $M^{+}_{0.72}[Si_{7.55}Al_{0.45}][Fe_{3.83}Mg_{0.05}]O_{20}(OH)_4$.

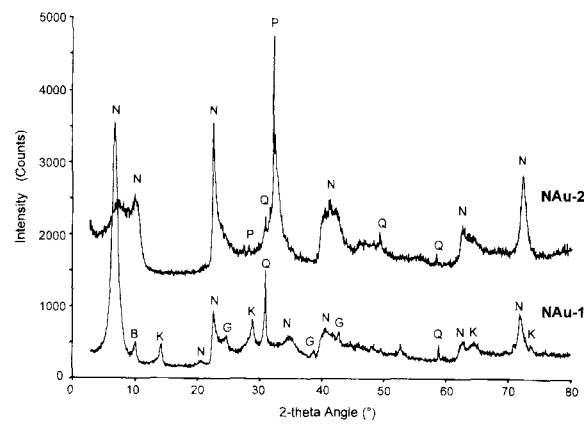

Figure 8. XRD traces of oven-dried bulk samples of NAu-1 and NAu-2. N-nontronite, P-calcic plagioclase, B-biotite, G-goethite, K-kaolin, Q-quartz.

https://doi.org/10.1346/CCMN.2000.0480506 Published online by Cambridge University Press

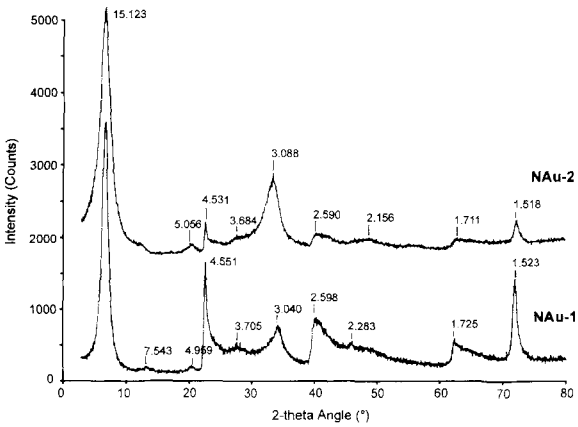

Figure 9. XRD traces of the <0.2-μm size fractions of NAu-1 and NAu-2.

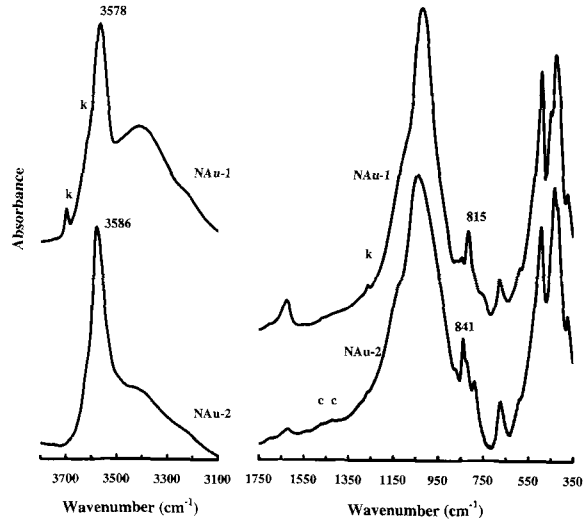

Figure 10. Selected regions of the mid infrared spectra of the <0.2-μm size fractions of NAu-1 and NAu-2. k-kaolin, c-carbonate.

Aluminum was assumed to fill available tetrahedral sites. However, individual analyses of some <0.2-μm size fractions of NAu-2 gave insufficient Al (Al_2O_3 < 2.5%) thereby suggesting that at least some Fe^{3+} occurs in tetrahedral coordination.

IR analyses

The IR spectra of the <0.2-μm size fractions for NAu-1 (Figure 10) showed that kaolin was present at 1–2% in all samples, suggesting that it was below the detection limit by XRD in some samples. Upon Li saturation, dialysis, and separation of the <0.15-μm size fraction (Goodman *et al.,* 1976), the kaolin was removed from NAu-1. Separation of the <0.15-μm fraction of NAu-2 resulted in an apparent increase in concentration (to ~1%) of a finely divided Mg/Mn-enriched carbonate responsible for bands at 2513, 1467, and 1417 cm^{-1} in diffuse reflectance infrared spectroscopy (DRIFT) spectra (Figure 10). The presence of carbonate was below detection by XRD. Subsequent treatment with 0.01 M acetic acid of a Na-saturated portion of this size fraction resulted in complete removal of the carbonate phase. Persistent trace amounts of an iron oxyhydroxide were inferred from a very weak band at 720 cm^{-1} in purified samples of NAu-2.

DISCUSSION

Clay distribution and nontronite formation

Clay minerals are a significant component of the rock mass at the Uley Mine. Throughout the 66-m core of drill hole MD 210, clay minerals average 45% by weight and below 50 m depth, where less weathering has occurred, clays average over 30% (Figure 3). Whereas deep weathering was significant in forming kaolin and iron oxide from primary metamorphic minerals, the distribution of nontronite suggests that nontronite alteration was not part of the weathering process.

The Cenozoic climatic history of southern Australia shows an overall trend of cooling and drying following the "greenhouse" conditions of the Cretaceous period. This trend was punctuated by episodes of warmer climate and high rainfall during the early Eocene and in the Miocene (Benbow, 1992) resulting in complex overprinting of weathering profiles that probably originated during the Cretaceous. Deep kaolinization of bedrock is common throughout the Gawler Craton, however, nontronite is rare. In particular, nontronite alteration in schist and gneiss has not been recognized. Even in weathered basic rocks on the Gawler Craton, nontronite is uncommon and, where present, it occurs as thin coatings on joint or fracture surfaces.

In MD 210, kaolin and iron oxides are dominant and pervasive in the upper 15 m of the drill core, and they have largely replaced all the alumino-silicate minerals. At depths deeper than ~15 m, remnants of primary minerals are present and kaolinization is either patchy or less intense and increasingly restricted to the product of feldspar alteration. The area of greatest ka-

Table 3. Major element data for <0.15-μm size fraction of NAu-1 and NAu-2 (ignited at 1050°C).

	SiO_2	TiO_2	Al_2O_3	Fe_2O_3	MgO	CaO	Na_2O	K_2O	Total
NAu-1	51.36	0.02	8.15	35.94	0.19	3.57	0.03	0.01	99.5
NAu-2	56.18	0.02	3.11	37.85	0.26	2.34	0.14	0.01	99.9

https://doi.org/10.1346/CCMN.2000.0480506 Published online by Cambridge University Press

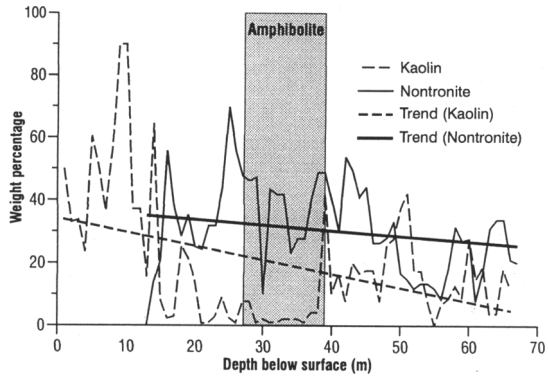

Figure 11. Kaolin and nontronite content *versus* depth for drill hole MD 210.

olinization in the upper part of the profile has been modified through displacement and replacement of quartz and kaolin by calcium carbonate precipitated within the vadose and upper phreatic zones, the result of mobilization of calcium ions from younger overlying calcarenite dunes. Disregarding this late influx of carbonate, the distribution of kaolin and iron oxides is consistent with deep weathering under high rainfall conditions and fluctuating or falling water table.

Comparison of the distribution of kaolin and nontronite in MD 210 indicates that nontronite has modified the kaolinization process. There is an general trend of decreasing kaolin content down the core (Figure 11) which correlates with increasingly obvious rock fabric and the appearance of garnet and K-rich feldspar at depth (Figure 3). This trend is modified between 14–38 m with lower than expected levels of kaolin despite the presence of biotite and plagioclase that easily weather. The interval corresponds with high nontronite levels which have clearly modified the intensity of kaolinization. Whereas nontronite content in MD 210 also shows some decline with depth, the trend is much less pronounced (Figure 11) and shows no apparent correlation with the weathering pattern.

Nontronite distribution occurs typically as veins concentrated in areas with a high degree of fracturing. Where irregular and diffuse patches of nontronite are present these are mostly adjacent to, or enclosed within, fracture networks involving nontronite veins. The structural setting and development of fractures appear to be significant controls on nontronite distribution, much more so than for kaolin.

The unusually high concentration of nontronite at Uley in what otherwise could be regarded as a typical deep kaolinized profile, the concentration of nontronite as veins in more fractured zones, the influence of nontronite to modify the intensity of kaolinization, plus the lack of any strong relationship between nontronite distribution and the weathering pattern, suggest that nontronite formed prior to deep weathering and was the alteration product of a low-temperature hydrothermal event associated with brittle fracturing.

The distribution of NAu-1 and NAu-2 is distinctive and reflects the conditions of formation. NAu-2 is essentially restricted to altered amphibolite where hornblende is observed at an advanced stage of dissolution. Ca-rich plagioclase in the same amphibolite is largely unaltered, showing only minor development of surface etch pits and no apparent kaolin alteration product. Nontronite is observed filling fracture and void spaces, and coating plagioclase grains. Remnants of hornblende grains typically show highly etched but clean surfaces, essentially free of smectite (Figure 7). Similar observations of amphibole dissolution have been reported by Berner and Schott (1982), Anand and Gilkes (1984), and Velbel (1989) and were interpreted as reflecting a relatively open hydrologic regime. A more closed system might produce smectite replacement of amphibole or pyroxene (*e.g.*, Eggleton, 1975; Banfield and Barker, 1993). At Uley, the pattern of NAu-2 distribution is consistent with brittle fracturing of the amphibolite and infiltration of fluid that preferentially dissolved hornblende (and pyroxene?) grains. This dissolution resulted in increased Fe and Si ions in solution that precipitated NAu-2 several centimeters distance.

NAu-1 is generally found as thin veins and is more likely to form diffuse patches enclosed by vein networks. Highest concentrations of NAu-1 are in fracture or shear zones, particularly in schistose units where original biotite content appears to have been high. NAu-1 was observed to have formed by alteration of individual biotite layers. NAu-1 contains almost three times more structural Al than NAu-2. High Al in green nontronite may result from direct incorporation of Al during replacement of biotite by nontronite. Alternatively, Al may have been incorporated through recrystallization of nontronite during later weathering and widespread kaolinization.

Nontronite purity and composition

Samples of NAu-1 and NAu-2 produced a high proportion of nontronite of uniform composition. Fine-grained impurities of kaolin in NAu-1 can be removed by taking a sample at <0.15 μm, but carbonate in NAu-2 requires dissolution with mild reagents. Traces of a fine-grained iron oxyhydroxide phase in NAu-2 were not completely removed. Impurities recognized by infrared analyses are not necessarily apparent from XRD.

The IR active vibrations for NAu-1 (<0.15-μm size fraction) are close to those of Garfield nontronite (Goodman *et al.*, 1976), and these two nontronites have similar chemical compositions. The position and intensity of bands assigned to $Fe_2(OH)$ librations, near 845 and 815 cm^{-1} in NAu-1, indicate that for NAu-1, the Fe^{3-} is mostly in the octahedral sheet, as is the

https://doi.org/10.1346/CCMN.2000.0480506 Published online by Cambridge University Press

case for most nontronite. Octahedral Al and Mg in NAu-1 are evident as weak bands near 870 and 786 cm^{-1}, assigned to FeAl(OH) and FeMg(OH), respectively (Figure 10).

IR spectrum of NAu-2 differs from NAu-1 in the relative intensity and position of $Fe_2(OH)$ librations: the higher frequency band is shifted by 4 cm^{-1} to 841 cm^{-1}, and the lower frequency band is less intense and shifted by 4 cm^{-1} to 819 cm^{-1} (Figure 10). These offset and intensity differences may be due to incomplete rehydration of the interlayer Ca^{2+} ions in NAu-2. The relatively strong OH librations at 872 and 790 cm^{-1} are consistent with FeAl(OH) and FeMg(OH) assignments, although the latter is better resolved than is typical (Goodman *et al.,* 1976), and may indicate an impurity. The intensity of the 872 cm^{-1} band in NAu-2 infers significant octahedral Al, despite their being barely enough Al to fill available tetrahedral sites (Table 3). Assignment of any Al to octahedral sites in NAu-2 therefore requires some Fe^{3+} be assigned to tetrahedral sites. An extension of this work into the use of IR bands to assign Fe to tetrahedral sites is currently being investigated.

ACKNOWLEDGMENTS

The authors acknowledge the assistance and advice of colleagues at CSIRO in the preparation and characterization of Uley nontronites, in particular P. Slade for clay separation and nontronite structure, S. McClure and P. Self (University of South Australia) for electron microscopy, and G. Riley for sample preparation. J. Weber (PIRSA) drafted Figures 1–3 and 11. Helpful comments on an early draft of this paper were made by J. Churchman and P. Self. The authors acknowledge also constructive reviews by R. April, R. Renaut, and S. Guggenheim. J. Keeling publishes with permission of the Director Mineral Resources, Primary Industry and Resources SA.

REFERENCES

Anand, R.R. and Gilkes, R.J. (1984) Weathering of hornblende, plagioclase and chlorite in meta-dolerite, Australia. *Geoderma,* **34,** 261–280.

Banfield, J.F. and Barker, W.W. (1993) Direct observation of reactant-product interfaces in natural weathering of exsolved, defective amphibole to smectite: Evidence for episodic, isovolumetric reactions involving structural inheritance. *Geochimica et Cosmochimica Acta,* **58,** 1419–1429.

Benbow, M.C. (1992) A review of past climate with emphasis on the recent past—a framework for the future. *Mines and Energy Review, South Australia,* **158,** 5–20.

Benbow, M.C., Callen, R.A., Bourman, R.P., and Alley, N.F. (1995) Deep weathering, ferricrete and silcrete. In *The Geology of South Australia. Volume 2, The Phanerozoic,* J.F. Drexel, and W.V. Preiss, eds., South Australia Geological Survey Bulletin 54, Adelaide, 201–207.

Bender Koch, C., Morup, S., Madsen, M.B., and Vistisen, L. (1995) Iron-containing weathering products of basalt in a cold, dry climate. *Chemical Geology,* **122,** 109–119.

Berner, R.A. and Schott, J. (1982) Mechanism of pyroxene and amphibole weathering II. Observation of soil grains. *American Journal of Science,* **282,** 1214–1231.

Besson, G., Bookin, A.S., Dainak, L.G., Rautereau, M., Tsipursky, S.I., Tchoubar, C., and Drits, V.A. (1983) Use of diffraction and Mössbauer methods for the structural and crystallochemical characterization of nontronites. *Journal of Applied Crystallography,* **16,** 374–383.

Bischoff, J.L. (1972) A ferroan nontronite from the Red Sea geothermal system. *Clays and Clay Minerals,* **20,** 217–223.

Bodine, M.W., Jr. (1987) CLAYFORM: A Fortran 77 computer program apportioning the constituents in the chemical analysis of a clay or other silicate mineral into a structural formula. *Computers and Geosciences,* **13,** 77–88.

Bonnin, D., Calas, G., Suquet, H., and Pezerat, H. (1985) Sites occupancy of Fe^{3+} in Garfield nontronite. A spectroscopic study. *Physics and Chemistry of Minerals,* **12,** 55–64.

Bradley, G.M. (1980) Metamorphism of the Archaean and Proterozoic basement at southern Eyre Peninsula. *Journal of the Geological Society of Australia,* **25,** 199–218.

Cardile, C.M. and Johnston, J.H. (1985) Structural studies of nontronites with different iron contents by ^{57}Fe Mössbauer spectroscopy. *Clays and Clay Minerals,* **33,** 295–300.

Drexel, J.F., Priess, W.V., and Parker, A.J. (1993) *The Geology of South Australia. Volume 1, The Precambrian.* Geological Survey of South Australia Bulletin 54, Adelaide, 242 pp.

Eggleton, R.A. (1975) Nontronite topotaxial after hedenbergite. *American Mineralogist,* **60,** 1063–1068.

Eggleton, R.A. (1977) Nontronite: Chemistry and X-ray diffraction. *Clay Minerals,* **12,** 181–194.

Goodman, B.A., Russell, J.D., Fraser, A.R., and Woodhams, F.W.D. (1976) A Mossbauer and I.R. spectroscopic study of the structure of nontronite. *Clays and Clay Minerals,* **24,** 53–59.

Köhler, B., Singer, A., and Stoffers, P. (1994) Biogenic nontronites from marine white smoker chimneys. *Clays and Clay Minerals,* **42,** 689–701.

Manceau, A., Chateigner, D., and Gates, W.P. (1998) Polarized EXAFS, distance-valance least-squares modelling (DLVS), and quantitative texture analysis approaches to the structural refinement of Garfield nontronite. *Physics and Chemistry of Minerals,* **25,** 347–365.

McNally, T.C. (1997) Uley graphite deposit. *MESA Journal,* **5,** 16–18.

Murad, E., Cashion, J.D., and Brown, L.J. (1990) Magnetic ordering in Garfield nontronite under applied magnetic fields. *Clay Minerals,* **25,** 261–269.

Murnane, R. and Clauge, D.A. (1983) Nontronite from a low-temperature hydrothermal system on the Juan de Fuca Ridge. *Earth and Planetary Science Letters,* **65,** 343–352.

Norrish, K. and Hutton, J.T. (1969) An accurate X-ray spectrographic method for the analysis of a wide range of geologic samples. *Geochimica et Cosmochimica Acta,* **33,** 431–451.

Parker, A.J. (1993) Palaeoproterozoic. In *The Geology of South Australia. Volume. 1, The Precambrian,* J.F. Drexel, W.V. Preiss, and A.J. Parker, eds., Geological Survey of South Australia Bulletin 54, Adelaide, 51–105.

Ross, C.S. and Hendricks, S.B. (1945) *Minerals of the Montmorillonite Group.* U.S. Geological Survey Professional Paper 205-B, Washington D.C., 23–79.

Taylor, J.C. (1991) Computer programs for standardless quantitative analysis of minerals using the full powder diffraction profile. *Powder Diffraction,* **6,** 2–9.

Taylor, J.C. and Matulis, C.E. (1994) A new method for Rietveld clay analysis. Part I. Use of a universal measured standard profile for Rietveld quantification of montmorillonites. *Powder Diffraction,* **9,** 119–123.

Taylor, W.R. and Berry, R.F. (1990) Origin of the Proterozoic graphite deposits of the southern Eyre Peninsula, South Australia—constraints from stable isotope geochemistry. In *Geological Society of Australia, 10th Australian Geological Convention, Hobart 1990, Abstracts,* 25, 230–231.

Velbel, M.A. (1989) Weathering of hornblende to ferruginous products by a dissolution-reprecipitation mechanism: Petrography and stoichiometry. *Clays and Clay Minerals,* **37,** 515–524.

Yeomans, J.C. and Bremer, J.M. (1991) Carbon and nitrogen analysis of soils by automated combustion techniques. *Communications in Soil Science and Plant Analysis,* **22,** 843–850.

E-mail of corresponding author: keeling.john@saugov.sa.gov.au

(Received 9 September 1999; accepted 27 April 2000; Ms. 377; A.E. Richard L. Hay)